Korean J. Chem. Eng., 37(4), 604-613 (2020)
DOI: 10.1007/s11814-020-0489-2

pISSN: 0256-1115
eISSN: 1975-7220

Numerical analysis on the performance of an SCR monolith reactor

Pengfei Feng, Ding Chen†, Yucheng Cao, and Yaotong Chen

State Key Laboratory of Advanced Design and Manufacturing for Vehicle Body, Hunan University, Changsha 410082, China
(*Received 22 August 2019 • accepted 9 January 2020*)

Abstract−An SCR catalyst is used as an example to investigate the effects of the washcoat diffusion limitation on the performance of monolith reactors. One-dimensional model and three-dimensional CFD model with and without washcoat diffusion limitation were established. The washcoat diffusion was modeled by using an effective diffusivity in the washcoat region (CFD modeling) and the internal mass transfer coefficient between the interface and the interior of the washcoat (One-dimensional modeling). The results show that numerical models with washcoat diffusion limitation give more accurate NO concentration prediction than the numerical models without washcoat diffusion limitation. Using the ratios of internal mass transfer resistance and reaction resistance to estimate the washcoat diffusion limitation, the correlation between the temperature and the washcoat limitation is discussed. Detailed comparisons of the 1-D model and CFD model are conducted.

Keywords: Monolith Reactor, SCR, Washcoat Diffusion, Mass Transfer, Numerical Modeling

INTRODUCTION

Catalytic monolith reactors are widely used in many engineering applications including selective catalytic reduction (SCR) reactors, three-way catalytic converter, steam reformation of hydrocarbons and catalytic combustion. A catalytic monolithic reactor with a honeycomb structure is comprised of numerous parallel channels [1]. A honeycomb shaped structure provides a catalytic reactor with both low pressure drops and high geometric surface areas per unit volume [2]. The channels of monolithic reactors are coated with a thin, microporous washcoat on the inner walls. As gaseous species flow through the channel, the species involved in the catalytic reactions diffuse into the washcoat and are adsorbed on the particles distributed in the washcoat. The reactions occur on the particles and the products undergo a desorption process and then diffuse back into the gaseous flow. Due to the complexity of the chemical and physical process, experimental tests alone cannot provide detailed information of the catalytic process and they are expensive and time-consuming. As a method to guide the optimization of catalytic monolithic reactors, numerical modeling becomes increasingly useful.

Various numerical models have been developed which can be categorized as one-dimensional (1-D) modeling, two-dimensional (2-D) modeling and three-dimensional (3-D) modeling. 1-D models use the concept of mass and heat transfer coefficient to simplify the complex mass and heat transport in monolith reactors. A number of studies on 1-D modeling have been conducted to study the mass transfer in monolith reactors [3-10]. 2-D and 3-D models are modeled using the Navier-Stokes equations coupled with the species diffusion equations, the reaction-diffusion balance equations and energy conservation equations, which can reveal detailed flow field information and transport phenomena within channels. However, a real physical size monolith reactor would consume tremendous amounts of computational time. Assuming that the mixture gas in all the channels of a monolith reactor undergoes the same physical and chemical process, most 2-D and 3-D numerical studies use a single channel to represent the whole reactor [11-20], including three-way catalytic converters [21-27], catalytic combustion [28-31] and steam reforming of methane [32-35]. In those works, computational fluid dynamics (CFD) codes coupled with surface and gas phase chemical reactions are used to establish the 2-D or 3-D models. To give a more detailed investigation of physical and chemical process in channels of monolith reactors, washcoat diffusion should not be ignored, especially when the pore size in washcoat is very small. Ashraf investigated the effects of washcoat thickness on the performance of catalytic reactors [36]. Rickenbach numerically investigated the effect of washcoat diffusion resistance on foam based catalytic reactors using a volume averaged reactor model [37]. Hayes et al. [38] employed an effectiveness factor to model the diffusion in washcoat using a one-dimensional model. Bhattacharya et al. [39] investigated the asymptotic mass-transfer coefficients within washcoat in monolith reactors with various cross-sectional shapes. Joshi et al. [40] studied the effect of flow rate, temperature, channel dimensions and washcoat properties on the performance of the monolith reactor considering washcoat diffusion limitation. Mladenov et al. [41] established a CFD model, boundary-layer model and one dimensional plug-flow model to evaluate the role of the washcoat diffusion limitation within washcoat in DOC. Irani et al. [42] established two CFD models for steam reforming of methane and compared the two different approaches, named surface approach, that did not consider washcoat diffusion limitation and volumetric approach considering washcoat diffusion limitation, and they concluded that the surface approach would have a more accurate prediction instead of the volumetric approach.

†To whom correspondence should be addressed.
E-mail: chending@hnu.edu.cn

Du et al. [43] commented that the reason for the inaccurate prediction of the volumetric approach is the underestimation of the active catalytic surface.

The objective of this work was to systematically investigate the effects of the washcoat diffusion limitation on the performance of the monolith reactor. To our knowledge, few studies on the comparison of 3-D and 1-D models for SCR reactors have been published. We used a Cu/SSZ-13 catalyst as an example, with smaller pore sizes within its washcoat compared to other kinds of catalysts. Besides, the ratio of internal mass transfer resistance and reaction resistance was calculated and used to estimate the washcoat diffusion limitation both for 3-D and 1-D models. Based on the 3-D and 1-D model, the effects of washcoat thickness on washcoat limitation were investigated and detailed comparisons for the 1-D model and 3-D model were conducted. The 3-D model was established using the commercial CFD code ANSYS Fluent 16.2 and the 1-D model was modeled using Matlab/Simulink (R2015b) code.

PHYSICAL MODEL

The single channel is presented in Fig. 1. The gaseous species diffuse from the gas flow to the interface between the gas phase and washcoat and then diffuse from the interface into the washcoat. The reactions occur within the washcoat and the products undergo an opposite diffusion process. The washcoat has average washcoat thickness of 40 μm.

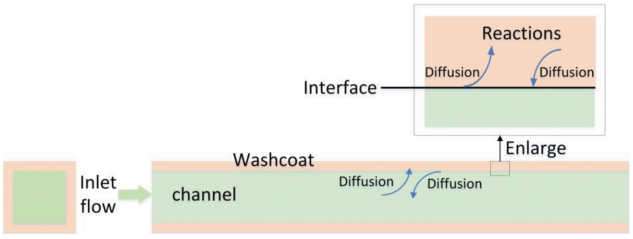

Fig. 1. Main physical and chemical process in the channel.

CFD MODELING

1. Governing Equations

In the present study, three-dimension Navier-Stokes equations were used to model the conservation of mass, momentum and energy in a single channel, giving detailed information of the species fraction, pressure and velocity in the flow field. The conservation of mass and momentum are as follows:

Conservation equation of mass:

$$\nabla(\rho\vec{v}) = 0 \tag{1}$$

Conservation equation of momentum:

$$\rho(\vec{v}\cdot\nabla\vec{v}) = -\nabla p + \nabla\cdot\left(\mu\left[\nabla\vec{v} + (\nabla\vec{v})^{T} - \frac{2}{3}\nabla\cdot\vec{v}I\right]\right) \tag{2}$$

Conservation equation of species mass:

$$\nabla(\rho\vec{v}Y_i) = -\nabla\cdot\vec{J}_i + R_i \tag{3}$$

where ρ is the gas density, $\vec{v}$ is the velocity, p is the static pressure, μ is the dynamic viscosity, I is the unit tensor, Y_i is the mass fraction of species *i*, $\vec{J}_i$ is the mass diffusion flux of species *i*, R_i is the production or consumption rate of the species *i* due to chemical reactions.

2. Modeling Chemical Reactions

The species involved in the SCR surface reactions include both the gas phase species and site species. The surface reaction mechanism can be written as the following [44]:

$$\sum_{i=1}^{N_g} g'_{i,r} G_i + \sum_{i=1}^{N_s} s'_{i,r} S_i \xleftrightarrow[k_{b,r}]{k_{f,r}} \sum_{i=1}^{N_g} g''_{i,r} G_i + \sum_{i=1}^{N_s} s''_{i,r} S_i \tag{4}$$

where G_i represents the gas phase species and S_i represents the site species or adsorbed species. N_g and N_s are the total numbers of these species. $g'_{i,r}$ and $s'_{i,r}$ are the stoichiometric coefficients for each reactant species *i*, $g''_{i,r}$ and $s''_{i,r}$ are the stoichiometric coefficients for each product species *i*. $k_{f,r}$ and $k_{b,r}$ are the forward and backward rate of reactions, respectively.

The surface reaction mechanism used in this study is taken from

Table 1. Reactions and the reaction rate expressions [45]

Reactions	Reaction rate	Number
$NH_3+S1\leftrightarrow S1-NH_3$	$r_{1f}=\rho_{S1}k_{1,f}y_{NH_3}\theta_{S1}$ $r_{1b}=\rho_{S1}k_{1,b}\theta_{S1-NH_3}$	(1)
$NH_3+S2\leftrightarrow S2-NH_3$	$r_{2f}=\rho_{S2}k_{2,f}y_{NH_3}\theta_{S2}$ $r_{2b}=\rho_{S2}k_{2,b}\theta_{S2-NH_3}$	(2)
$NH_3+S3\leftrightarrow S3-NH_3$	$r_{3f}=\rho_{S3}k_{3,f}y_{NH_3}\theta_{S3}$ $r_{3b}=\rho_{S3}k_{3,b}\theta_{S3-NH_3}$	(3)
$2S1-NH_3+1.5O_2\rightarrow N_2+3H_2O+2S1$	$r_4=\rho_{S1}k_4y_{O_2}^{0.6}\theta_{S1-NH_3}$	(4)
$2S2-NH_3+1.5O_2\rightarrow N_2+3H_2O+2S2$	$r_5=\rho_{S2}k_5y_{O_2}^{0.6}\theta_{S2-NH_3}$	(5)
$4S1-NH_3+4NO+O_2\rightarrow 4N_2+6H_2O+4S1$	$r_6=\rho_{S1}k_6y_{NO}y_{O_2}^{0.5}\theta_{S1-NH_3}$	(6)
$4S2-NH_3+4NO+O_2\rightarrow 4N_2+6H_2O+4S2$	$r_7=\rho_{S2}k_7y_{NO}y_{O_2}^{0.5}\theta_{S2-NH_3}$	(7)
$S2-NH_3+NO\rightarrow S2-NH_3-4NO$	$r_{8f}=\rho_{S2}k_{8,f}y_{NO}\theta_{S2-NH_3}$ $r_{8b}=\rho_{S2}k_{8,b}\theta_{S2-NH_3-NO}$	(8)
$2S2-NH_3-NO+O_2\rightarrow N_2O+N_2+3H_2O+2S2$	$r_9=\rho_{S2}k_9y_{O_2}\theta_{S2-NH_3-NO}$	(9)
$2S2-NH_3+2NO+O_2\rightarrow N_2O+N_2+3H_2O+2S2$	$r_{10}=\rho_{S2}k_{10}y_{O_2}\theta_{S2-NH_3}$	(10)

Olsson and is expressed in Table 1 [45]. The mechanism consists of three reversible reaction and seven irreversible reactions. three gas-phase species, seven site species (or adsorbed species) are involved in the reactions. In Table 1, S1, S2 and S3 represent the three kinds of sites for ammonia adsorption, k_f and k_b are the rate constant for the forward and backward reaction, respectively, ρ_{S1}, ρ_{S2} and ρ_{S3} are the site density for the three kinds of sites, respectively, y_{NH_3} is the mole fraction of ammonia, θ_{S-NH_3} is the coverage of ammonia on the sites and θ_S is the fraction of the sites that is not covered by ammonia.

3. Modeling Diffusion

3-1. Modeling Diffusion in the Channel

The mass diffusion in the channel can be modeled by concentration gradient using Fick's diffusion law:

$$J_i = -\rho D_i \nabla Y_i - D_{T,i} \nabla T/T \tag{5}$$

where D_i is the mass diffusivity for species *i*, $D_{T,i}$ is the thermal (Soret) diffusion coefficient.

3-2. Modeling Diffusion in Washcoat

Porous media in flows can be modeled by adding a momentum source term to the standard fluid flow equations. The source term consists of a viscous loss term and an inertial loss term, causing a pressure drop that is proportional to the fluid velocity. The source term for a homogeneous porous media can be expressed as

$$S_i = -\left(\frac{\mu}{a} v_i + C_2 \frac{1}{2} \rho |v| v_i\right) \tag{6}$$

where a is the permeability, μ is the dynamic viscosity and C_2 is the inertial resistance factor.

An effective diffusivity was applied to model the mass diffusion in porous region. Taking the bulk diffusion and Knudsen diffusion into consideration, the effective diffusivity D_{eff} can be expressed as [46]:

$$\frac{1}{D_{eff}} = \frac{\tau}{\varepsilon}\left(\frac{1}{D_i} + \frac{1}{D_{kund,i}}\right) \tag{7}$$

where ε is the porosity of washcoat and τ is the tortuosity.

The Knudsen diffusion coefficient of species *i* can be given as

$$D_{kund,i} = \frac{d_p}{3}\sqrt{\frac{8RT}{\pi M_i}} \tag{8}$$

where d_p is the average pore diameter in the washcoat, R is the ideal gas constant, T is the temperature and M_i is the molecular mass of species *i*. The average pore diameter d_p is set to 4 nm, which is a common pore size for SSZ-13 zeolites [47]. The tortuosity τ is commonly in the range of 3-5 and is set to 4 in this study [48]. The washcoat porosity ε ranges from 0.4 to 0.6 and the value of 0.4 is used in this study [49-51]. The expression for the temperature dependent diffusivity of NO is $D_i = 1.2365 \times 10^{-9} T^{1.7006}$ [52]. By using the user defined functions (UDF) in Fluent, the effective diffusivity D_{eff} is loaded in the diffusion equation.

4. Diffusion Reaction Balance Equation

Both the CFD models with and without washcoat diffusion limitation assume that the reactions occur on the surface. The CFD model without washcoat diffusion limitation assumes that the reactions occur at the interface between the washcoat and the gas phase. While, the CFD model with washcoat diffusion limitation assumes that the reactions occur at the surface of the micropores within the washcoat. Both of them can be described by the same equations. For gas species, the mass flux of each gas species due to diffusion to the surface is equal to the rate of production or consumption considering the catalytic surface area due to surface chemical reactions. At a steady-state process, the Stefan velocity vanishes unless etching or mass deposition exists on the surface. Therefore, the balance equation can be written as [22]:

$$\rho D_i \frac{\partial Y_{i,s}}{\partial n} = M_i R_i F_{cat/geo} \tag{9}$$

where $Y_{i,s}$ is the mass fraction on the surface, $F_{cat/geo}$ is the ratio of catalytic surface area to geometric surface area.

For site species, the time-dependent site coverage of species *i* can be modeled by [22]:

$$\rho_{site} = \frac{\partial \theta_i}{\partial t} = R_{i,site} \tag{10}$$

where f is the site density, θ_i is the site coverage for species *i* and $R_{i,site}$ is the net consumption or production rate of site species *i*.

1-D MODELING

1. 1-D Modeling without Washcoat Diffusion Limitation

For 1-D modeling without washcoat diffusion limitation, the catalytic reactions are assumed to occur on the interface between the gas phase and the washcoat. The external mass transfer coefficient k_{me} is used to model the diffusion from the gas phase to the interface. Assuming that the velocity and the cross section area are constant, the transient gas phase equation can be modeled by [53]:

$$\varepsilon_m \frac{\partial C_{g,i}}{\partial t} + \varepsilon_m u \frac{\partial C_{g,i}}{\partial x} = -k_{me} G_a (C_{g,i} - C_{f,i}) \tag{11}$$

where ε_m is the porosity of the monolith reactor, u is the velocity of the gas phase, $C_{g,i}$ is the average concentration of the gas phase species *i*, $C_{f,i}$ is the concentration of the species *i* on the interface, k_{me} is the external mass transfer coefficient, G_a is the geometric surface area-to-volume ratio for the monolith reactor.

The mass flux of the gas phase species *i* to the surface is balanced by the consumption of the species *i*. The species equation on the interface can be written as [53]:

$$k_{me}(C_{g,i} - C_{f,i}) = F_{cat/geo} R_i \tag{12}$$

The external mass transfer coefficient k_{me} can be given by:

$$k_{me} = \frac{Sh_e D_i}{4R_\Omega} \tag{13}$$

where R_Ω is effective average diffusion length and is defined by the ratio of the area to the perimeter of monolith channels and the Sherwood number Sh_e is given by the following correlation [54]:

$$Sh_e = \begin{cases} 1.007(fRe)^{1/3} P^1 & \text{for } P > \dfrac{0.8 Sh_{e\infty}^3}{fRe} \\ Sh_{e\infty} & \text{for } P \le \dfrac{0.8 Sh_{e\infty}^3}{fRe} \end{cases} \tag{14}$$

where P is the transverse Peclet number, f is the friction factor, Re is Reynolds number.

Considering the SCR reaction mechanism used in this study, the reaction rate of the NO reduction can be written as

$$R_{NO}=k_{NO}C_{f,NO}Z_{NH_3}\theta_{NH_3} \quad (15)$$

where Z_{NH_3} is the site density for adsorbing NH_3, $C_{f,NO}$ is the concentration of NO on the interface, θ_{NH_3} is the coverage of NH_3 and the rate constant k_{NO} is given by the Arrhenius equation:

$$k_{NO}=Ae^{-E_a/RT} \quad (16)$$

The coverage of NH_3 is time dependent and can be expressed by

$$Z_{NH_3}\cdot\frac{\partial\theta_{NH_3}}{\partial t}=R_{NH_3} \quad (17)$$

here, R_{NH_3} is the net adsorption rate of NH_3 on the interface.

2. 1-D Modeling with Washcoat Diffusion Limitation

For 1-D modeling with washcoat diffusion limitation, the diffusion process is divided into two stages: diffusion from the gas phase to the interface and diffusion from the interface into the washcoat. The equation used to describe the diffusion from the gas phase to the interface is same as the 1-D modeling without washcoat diffusion limitation, which has been expressed in Eq. (11). The mass flux due to the diffusion from the gas phase to the interface is equal to the mass flux due to diffusion from the interface into the washcoat [55]:

$$k_{me}(C_{g,i}-C_{f,i})=k_{mi}(C_{f,i}-C_{w,i}) \quad (18)$$

where, k_{mi} is the internal mass transfer coefficient for species *i* and $C_{w,i}$ is the volume averaged concentration of species *i* in the washcoat.

The mass flux of species from the interface to the washcoat is balanced by the consumption of the species due to reactions [55]:

$$k_{mi}(C_{f,i}-C_{w,i})=F_{cat/geo}R_i \quad (19)$$

where $C_{w,i}$ is the volume averaged concentration of species *i* within the washcoat.

The consumption rate of NO considering the ratio of catalytic surface area to geometric surface area in the washcoat and can be expressed as

$$F_{cat/geo}R_{NO}=F_{cat/geo}k_{NO}C_{w,NO}Z_{NH_3}\theta_{NH_3}=k_vL_cC_{w,NO} \quad (20)$$

where k_v is a rate based on washcoat volume, the characteristic length L_c is defined as the ratio of catalyst volume to surface area. The balance Eq. (19) for NO can be expressed as:

$$k_{mi}(C_{f,NO}-C_{w,NO})=k_vL_cC_{w,NO}=kC_{w,NO} \quad (21)$$

$$k=k_vL_c \quad (22)$$

The internal mass transfer coefficient can be given by

$$k_{mi}=\frac{Sh_iD_{eff}}{L_c} \quad (23)$$

where the internal Sherwood number Sh_i is defined by [56]:

$$Sh_i=Sh_{i\infty}+\frac{\Lambda\phi^2}{1+\Lambda\phi} \quad (24)$$

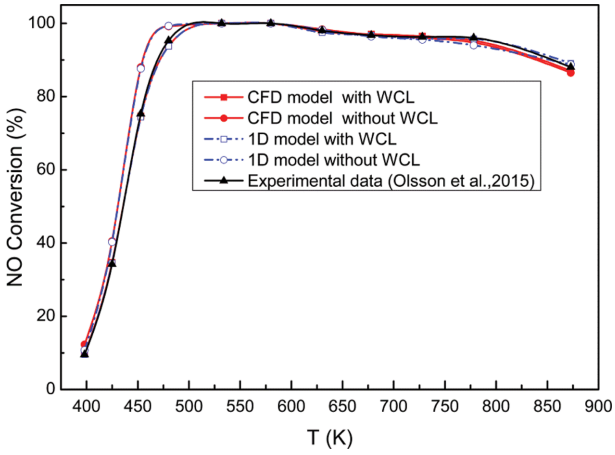

Fig. 2. Comparison of NO conversion for CFD models with and without WCL (washcoat diffusion limitation) and 1-D models with WCL and without WCL.

where Λ is a constant that depends on the washcoat geometry and ϕ is the Thiele modulus. For a first-order reaction in concentration, the Thiele modulus is expressed as [57]:

$$\phi=L_c\sqrt{\frac{k_v}{D_{eff}}} \quad (25)$$

RESULTS AND DISCUSSION

1. Comparison of the CFD Model and 1-D Model

1-1. Comparison of the NO Conversion at the Outlet

Fig. 2 shows the comparison of the CFD models and 1D models with and without washcoat diffusion limitation, and the numerical results are compared with the experimental data of Olsson et al. [45]. The inlet flow rate and gas temperature for the CFD models and 1D models are according to the inlet boundary condition of the monolith reactor in Olsson's experiment. The mixture gas with an inlet flow of 3,500 ml min^{-1} leads to a space velocity of 30,300 h^{-1}. The 400 cpsi monolith reactor with 20 mm in length and 21 mm in diameter is modeled in 1-D model. While for the CFD model, a single channel of the monolith reactor is taken into consideration to represent the whole reactor.

The CFD model and 1-D model with washcoat diffusion limitation give a more accurate prediction of the NO conversion compared to the CFD model and 1-D model without washcoat diffusion limitation. Both the CFD model and 1-D model without washcoat diffusion limitation overestimate the NO conversion. At 398 K, there is little difference between the four models. As the temperature increases from 398 K to 453 K, the differences of the NO conversion between the numerical models with and without washcoat diffusion limitation increase. As the temperature increases from 453 K to 580 K, the differences of the NO conversion between the numerical models with and without washcoat diffusion limitation decrease. As the temperature increases from 580 K to 873 K, the NO conversion efficiency decreases due to the oxidation of NH_3 at the elevated temperatures. Furthermore, the NO conversion efficiency shows little difference between the models with and without washcoat limitation at temperatures from 580 K to 873 K.

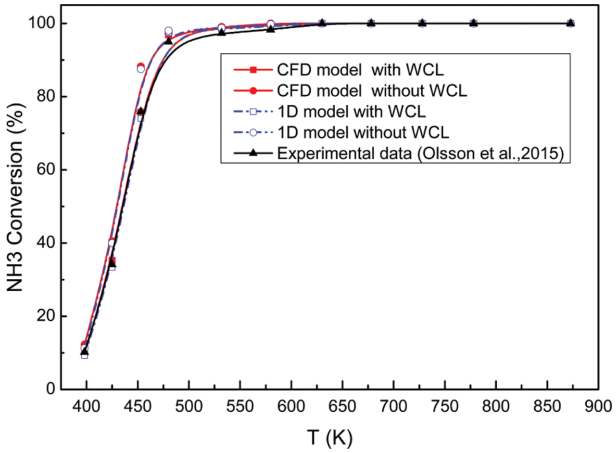

Fig. 3. Comparison of NH_3 conversion for CFD models with and without WCL and 1-D models with WCL and without WCL.

1-2. Comparison of the NH_3 Conversion at the Outlet

Fig. 3 shows the comparison of the CFD models with and without washcoat diffusion limitation for NH_3 conversion. The conversion of NH_3 is similar to the conversion of NO at a temperature below 678 K. From 678 K to 873 K, the oxidation of NH_3 becomes increasingly significant and the consumption of NH_3 is composed of the reduction by NO and the oxidation of NH_3.

1-3. Comparison of the NO Concentration Along the Axis Direction

Fig. 4 shows the concentration distribution of the NO obtained by CFD models with and without washcoat diffusion limitation. The contour of CFD models at 425 K, 453 K and 480 K with washcoat diffusion limitation presents a strong concentration gradient near the wall due to the existence of the washcoat, which indicates that the washcoat diffusion limitation should not be neglected. However, at 398K, the contour of concentration for the two models cannot even be distinguished and the concentration gradient near the wall is not obvious.

Figs. 5, 6, 7 and 8 show the comparison of the CFD models with and without washcoat diffusion limitation and 1-D models with and without washcoat diffusion limitation at 398 K, 425 K, 453 K and 480 K. The CFD model with washcoat diffusion limitation and

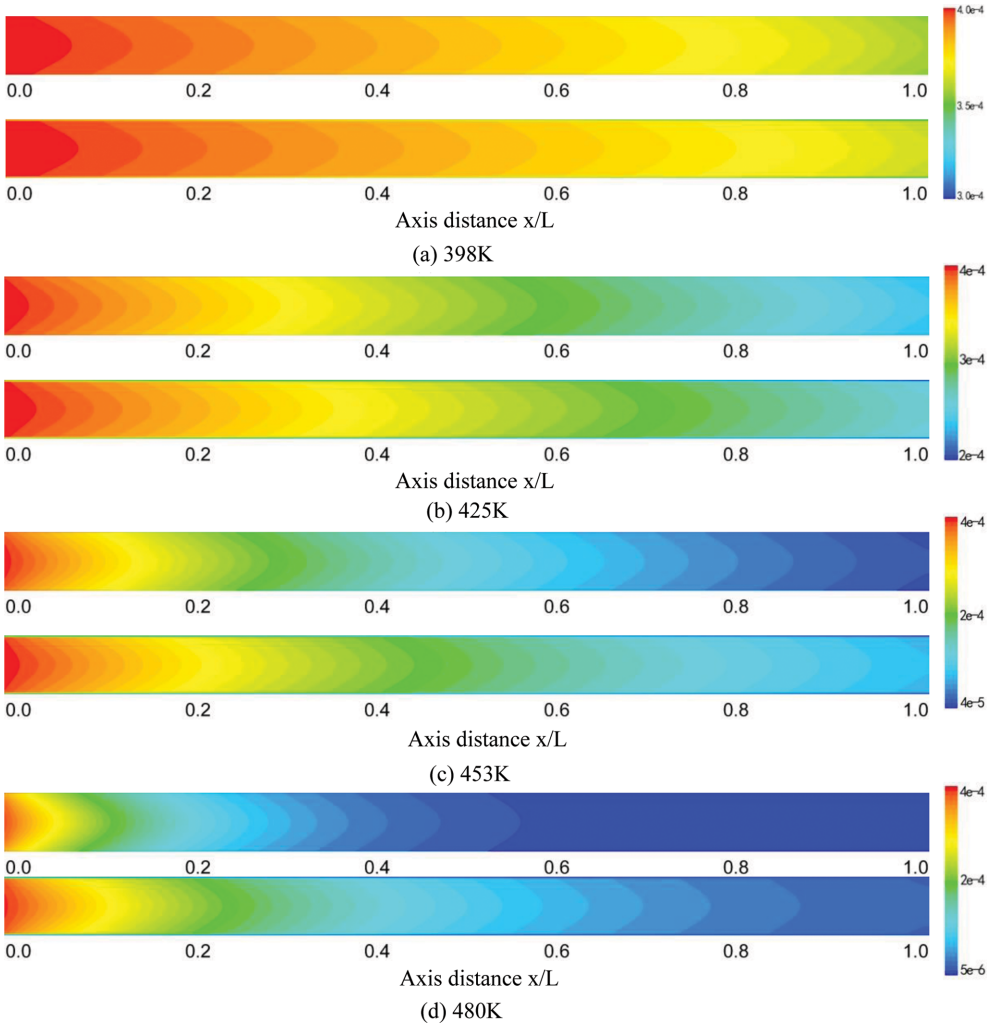

Fig. 4. Contours of concentration of NO at 398 K, 425 K, 453 K and 480 K: The upper is obtained by CFD models without washcoat diffusion limitation and the lower is obtained by CFD models with washcoat diffusion limitation.

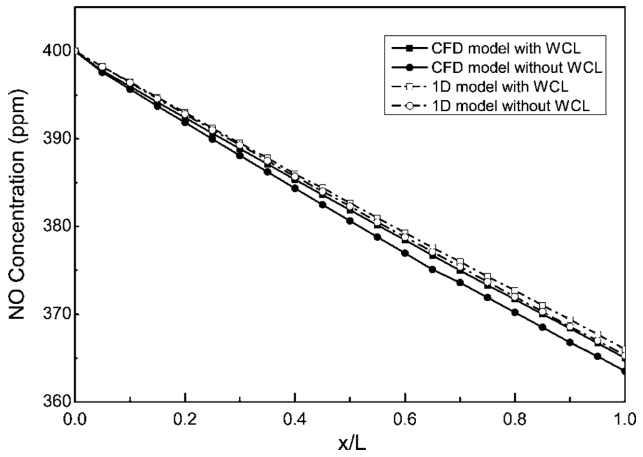

Fig. 5. Comparison of the CFD models with and without WCL (washcoat diffusion limitation) and 1-D models with and without WCL at 398 K.

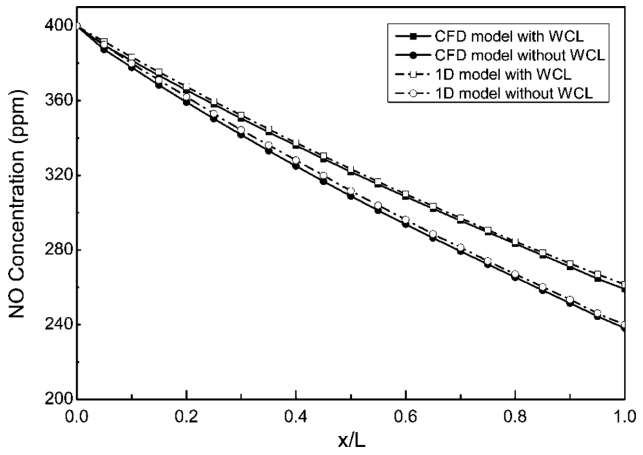

Fig. 6. Comparison of the CFD models with and without WCL (washcoat diffusion limitation) and 1-D models with and without WCL at 425 K.

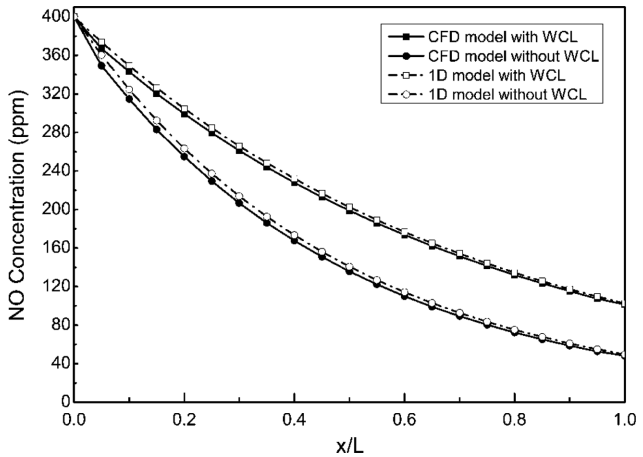

Fig. 7. Comparison of the CFD models with and without WCL (washcoat diffusion limitation) and 1-D models with and without WCL at 453 K.

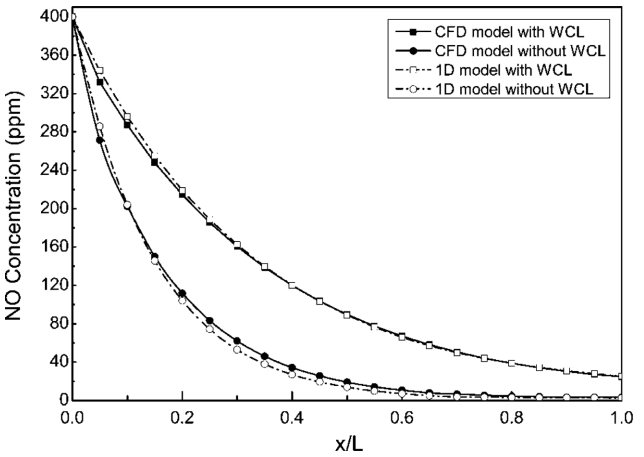

Fig. 8. Comparison of the CFD models with and without WCL (washcoat diffusion limitation) and 1-D models with and without WCL at 480 K.

1-D model with washcoat diffusion limitation give similar predictions of the NO conversion and NO concentration along the channel. The maximum difference of the NO concentration along the channel at 398 K, 425 K, 453 K and 480 K for the two kinds of models is 1 ppm, 2 ppm, 7 ppm and 12 ppm, respectively.

The maximum difference of the NO concentration along the channel for the CFD models and 1-D models occurs at the position of x/L=0.05, close to the inlet. The main reason is that the 1-D models neglect axial diffusion in the axial direction and the diffusion in channels is only radically dependent and is modeled by the functions of the radial geometric dimensions of the channel and washcoat. While, based on the Navier-Stokes equations, the CFD models solve a set of mass conservation equations in x, y, and z direction. Hence, axial diffusion is included in the models. As shown in Fig. 3, the increasing temperature results in an increasing axial gradient of NO near the inlet of the channel, which can induce considerable axial diffusion in the channel. This can explain the difference of the NO concentration near the inlets for the 1-D models and CFD models as the temperature is high.

Comparing the four models with and without washcoat diffusion limitation, both the NO conversion and NO concentration along the channel show little difference at 398 K, which proves that at low temperature, the washcoat diffusion limitation has little effect on NO conversion. As the temperature increases from 398 K to 453 K, the washcoat diffusion limitation shows an increasingly significant effect on the NO conversion and the NO concentration along the channel. As the temperature increases from 453 K to 480 K, the difference of NO conversion between the numerical models with and without WCL decreases. This is because the NO conversion is approaching 100% at high temperature. Taking the NO concentration along the channel into consideration, it could be observed that the NO concentration of the numerical models with and without washcoat limitation along the channel at 480 K show even more difference along the channel. At 480 K, the maximum difference of the NO concentration along the channel for numerical models with and without washcoat diffusion limitation exceeds 100 ppm at x/L=0.2 and 0.25, respectively. By contrast, the

maximum difference for the models with and without washcoat diffusion limitation is within 2 ppm at 398 K.

2. The Internal Mass Transfer Resistance and Reaction Resistance

Using the concepts of internal mass transfer resistance R_i ($R_i=1/k_{mi}$) and reaction resistance R_r ($R_r=1/k$), the effects of the washcoat diffusion limitation on the performance of monolith reactors can be evaluated by the concentration ratio [40]. Eq. (26) which is derived from Eq. (21) gives a criterion to evaluate the effects of the washcoat diffusion limitation on the NO conversion.

$$\frac{R_i}{R_r}=\frac{C_{f,NO}-C_{w,NO}}{C_{w,NO}}=\frac{C_{f,NO}}{C_{w,NO}}-1 \tag{26}$$

The internal mass transfer resistance is expressed as

$$R_i=\frac{L_c}{Sh_i D_{eff}} \tag{27}$$

The reaction resistance is expressed as

$$R_r=\frac{1}{k}=\frac{1}{F_{cat/geo}k_{NO}Z_{NH_3}\theta_{NH_3}} \tag{28}$$

Fig. 9 shows the ratios of internal mass transfer resistance and reaction resistance (R_i/R_r) at 398 K, 425 K, 453 K and 480 K, respectively. The values of R_i/R_r obtained from the 1-D model are close to the values from the CFD model, which confirms the validation of the 1-D model for evaluating the internal mass transfer resistance and reaction resistance. Note that the values of R_i/R_r almost maintain a constant value along the channel at 398 K, 425 K and 453 K, while the values of R_i/R_r decrease as x/L exceeds 0.55 at 480 K. The reason is that the decrease of the coverage of NH_3 (θ_{NH_3}) due to reactions leads to the decrease of the k ($k=F_{cat/geo}k_{NO}Z_{NH_3}\theta_{NH_3}$), resulting in the increase of R_r.

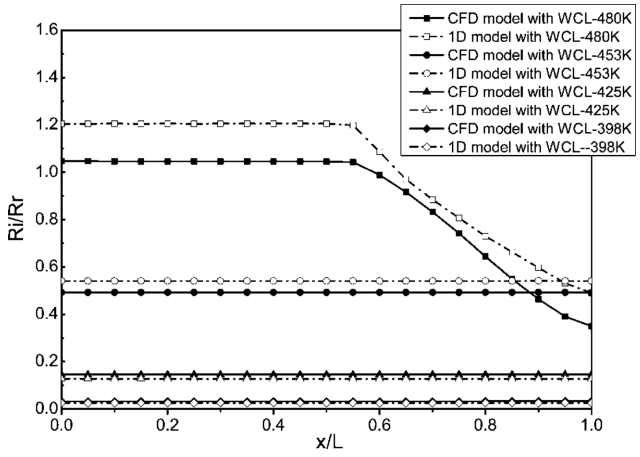

Fig. 9. Ratios of internal mass transfer resistance and reaction resistance at 398 K, 425 K, 453 K and 480 K.

The values of R_i/R_r increase with the temperature increasing from 398 K to 480 K. A small value of R_i/R_r means that the reaction resistance has a more significant effect on the performance of the monolith reactor. An increasing value of R_i/R_r means that the internal mass transfer resistance plays an increasingly important role, resulting in a stronger washcoat diffusion limitation.

Fig. 10 shows the mass fraction gradient within the washcoat and the NO concentration at the same place in the washcoat at 425 K, 453 K and 480 K (t represents the thickness of the washcoat). The mass fraction gradient is obtained by UDF in Fluent software. It could be observed that the mass fraction gradient in the washcoat increases with the increasing temperature. A strong mass fraction gradient exists in the washcoat at 480 K, while the NO concentration is small. A weak mass fraction gradient exists in the washcoat at 398 K but the NO concentration is the largest.

Fig. 9 can be used to explain Eq. (26). At low temperature (T= 398 K), the reaction rate is slow and the consumption of the reactants due to the reactions is very small. Therefore, a small mass flux of the reactants exists between the interface and the washcoat, which results in a small concentration gradient between the interface and washcoat. In this case, the value of the $C_{f,NO}$ and $C_{w,NO}$ is much close and the value of R_i/R_r is very small and the washcoat diffusion limitation is negligible. As the temperature increases, the reaction rate becomes faster and the consumption of the reactants involved in the reaction increases. Hence, a large mass flux of the reactants exists between the interface and the washcoat, which results in a larger concentration gradient between the interface and washcoat. A larger concentration gradient means that $C_{w,NO}$ is very small compared to $C_{f,NO}$ and is greatly affected by the washcoat diffusion limitation. While, $C_{w,NO}$ is directly related to the reaction

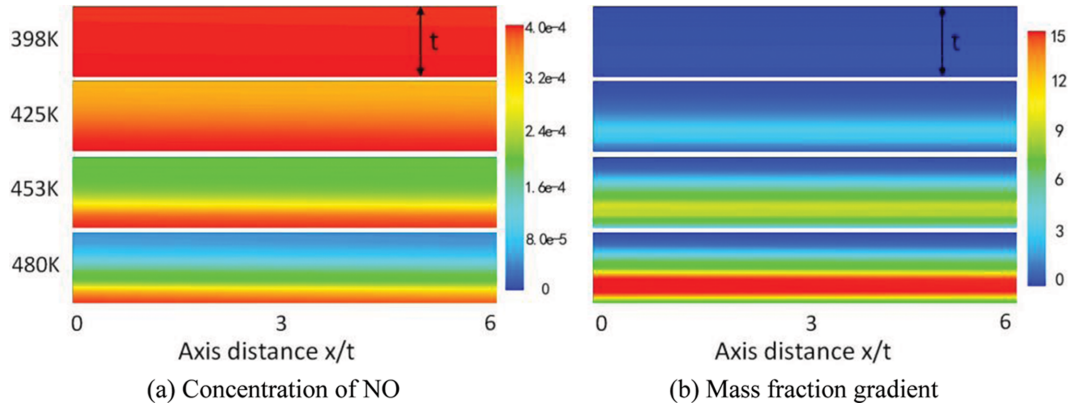

Fig. 10. Contours of the concentration of NO (a) and the mass fraction gradient of NO (b) at 398 K, 425 K, 453 K and 480 K, respectively.

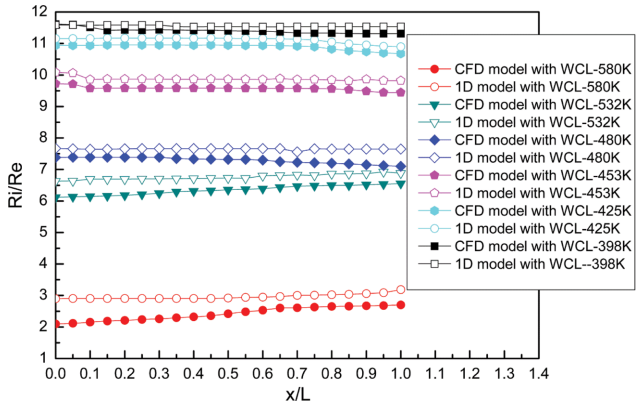

Fig. 11. Ratios of internal and external mass transfer resistance.

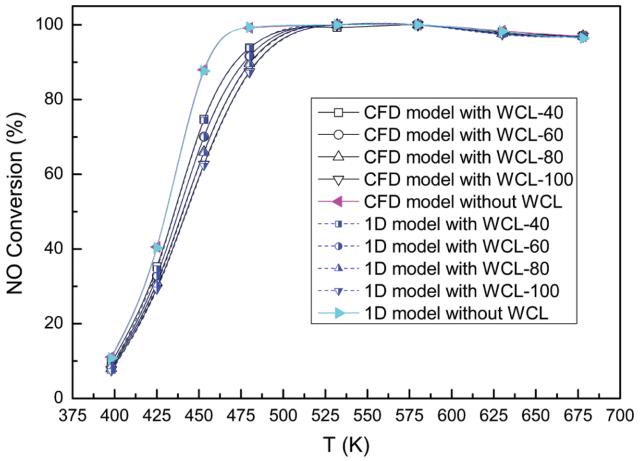

Fig. 12. Comparison of NO conversion for CFD models and 1-D models with washcoat thickness of 40, 60, 80 and 100 μm respectively.

rate of the NO reduction. Eventually, the washcoat diffusion limitation would have an increasingly significant effect on NO conversion.

3. The External Mass Transfer Resistance

The ratio of the internal and external mass transfer resistance can be used to evaluate the effects of the external mass transfer resistance on reactors. It can be computed by:

$$\frac{R_i}{R_e} = \frac{C_{f,NO} - C_{w,NO}}{C_{g,NO} - C_{f,NO}} \tag{29}$$

The external mass transfer resistance is expressed as:

$$R_e = \frac{1}{k_{me}} = \frac{4R_\Omega}{Sh_e D_i} \tag{30}$$

Fig. 11 shows the ratios of internal mass transfer resistance and external mass transfer resistance (R_i/R_e) at 398 K, 425 K, 453 K, 480 K, 532 K and 580 K, respectively. The values of R_i/R_e obtained from the 1-D model are close to the values from the CFD model, and the values of R_i/R_e do not change much along the channel at a given temperature. The values of R_i/R_e decrease with the increasing temperature from 398 K to 580 K. At 398 K, the internal mass transfer resistance is about ten-times the external mass transfer resistance. While at 580 K, the internal mass transfer resistance is about two- to three-times the external mass transfer resistance and the effect of external mass transfer resistance on reactor performance is non-negligible.

4. Effects of Washcoat Thickness on NO Conversion and Washcoat Limitation

4-1. Effects of Washcoat Thickness on NO Conversion

By assuming that the washcoat with various thickness has the same number of sites for NH_3 adsorption, the effects of the washcoat thickness on the washcoat limitation can be evaluated. Fig. 12 shows the comparison of NO conversion for the CFD models and 1-D models with washcoat thickness of 40, 60, 80 and 100 μm, respectively. At 425 K to 480 K, the increase of the washcoat thickness results in the decrease of the NO conversion efficiencies, meaning the increasing effects of washcoat limitation. At 453 K, the NO conversion efficiency for the reactors with washcoat thickness of 40, 60, 80 and 100 μm is 74.7%, 70.1%, 66%, and 62.6%, respectively. At 532 K to 678 K, the NO conversion shows little difference

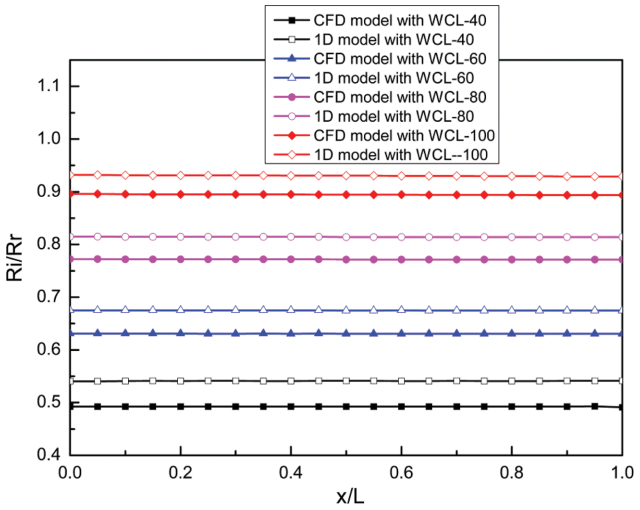

Fig. 13. Ratios of internal mass transfer resistance and reaction resistance at 453 K for reactors with washcoat thickness of 40, 60, 80 and 100 μm respectively.

since the exhaustion of NH_3 would terminate the NO reduction reactions.

4-2. Effects of Washcoat Thickness on Washcoat Limitation

Fig. 13 shows the ratios of internal mass transfer resistance and reaction resistance (R_i/R_r) at 453 K for the reactors with washcoat thickness of 40, 60, 80 and 100 μm, respectively. Corresponding to the NO conversion efficiency for the reactors with washcoat thickness of 40, 60, 80 and 100 μm, the ratios of internal mass transfer resistance and reaction resistance increase with the increase of the washcoat thickness.

CONCLUSION

Numerical models, including CFD models with and without washcoat diffusion limitation and 1-D models with and without washcoat diffusion limitation, were developed and compared with

each other. The washcoat diffusion was modeled using an effective diffusivity in the washcoat region (CFD modeling) and the internal mass transfer coefficient between the interface and the interior of the washcoat (1-D modeling).

Both the CFD model and 1-D model without washcoat diffusion limitation overestimate the NO conversion, which confirms that the effects of the washcoat diffusion limitation on NO conversion should not be ignored. The differences between the numerical models with and without washcoat diffusion limitation increase with the increasing temperature, which indicates that the temperature would affect the effects of the washcoat diffusion limitation on the NO conversion.

The ratios of internal mass transfer resistance and reaction resistance (R_i/R_r) can be used to evaluate the effects of washcoat diffusion limitation on the NO conversion. The values of R_i/R_r obtained from the 1-D model are close to the values from the CFD model, which confirms the validation of the 1-D model for evaluating the internal mass transfer resistance and reaction resistance. The CFD model and 1-D model give a similar prediction of the external mass transfer resistance. The ratios of internal mass transfer resistance and external mass transfer resistance (R_i/R_e) are small and decrease with the increasing temperature. As the temperature increases, the effect of external mass transfer resistance becomes increasingly significant.

As computational tools to study the performance of the monolith reactor, both the CFD model and 1-D model can obtain satisfactory predictions of the conversion of the species. The difference of the computed values is mainly due to the different equations used in the 1-D and CFD model. The 1-D model does not consider the axial diffusion in the axial direction, and the diffusion in channels is modeled by the functions of the radial geometric dimensions of channels and washcoat. The CFD models solve a set of mass conservation equations in x, y, and z direction including both the axial diffusion and radical diffusion. This may lead to a non-negligible difference between the two models at the region where the axial concentration gradient is larger.

The CFD model is computationally expensive but can provide more detailed information. The 1-D model is computationally efficient but cannot reveal the detailed transport phenomena. Moreover, the 1-D model needs to choose or calculate the parameters such as Thiele modulus and the internal Sherwood number carefully, since they are determined by complicated empirical formulas.

NOMENCLATURE

ρ : gas density
$\vec{v}$: velocity vector
p : static pressure
μ : dynamic viscosity
I : unit tensor
Y_i : mass fraction of species *i*
$\vec{J}_i$: mass diffusion flux of species *i*
R_i : production or consumption rate of the species *i* due to chemical reactions
D_i : mass diffusivity for species *i*
$D_{T,i}$: thermal (Soret) diffusion coefficient
S_i : momentum source term
a : permeability
C_2 : inertial resistance factor
D_{eff} : effective diffusivity
v_i : velocity
$|v|$: magnitude of the velocity
$D_{kund,i}$: Knudsen diffusion coefficient of species *i*
d_p : average pore diameter for the washcoat
R : ideal gas constant
T : temperature
M_i : molecular mass of species *i*
$F_{cat/geo}$: ratio of catalytic surface area to geometric surface area
ρ_{site} : site density
$R_{i,site}$: net consumption or production rate of site species *i*
u : velocity of gas phase
$C_{g,i}$: average concentration of the gas phase species *i*
G_a : geometric surface area-to-volume ratio for monolith reactors
k_{me} : external mass transfer coefficient
$C_{f,i}$: concentration of the species *i* on the interface
R_Ω : ratio of the area to the perimeter of monolith channels
Sh_e : Sherwood number
$Sh_{e\infty}$: asymptotic external Sherwood number
P : transverse Peclet number
Re : Reynolds number
f : friction factor
Z_{NH_3} : site density for adsorbing NH_3
θ_{NH_3} : coverage of NH_3
k_{NO} : rate constan for the NO reduction reaction
A : pre-exponential factor
E_a : activation energy
R : universal gas constant
k_{mi} : internal mass transfer coefficient for species *i*
Sh_i : internal Sherwood number
$C_{w,i}$: volume averaged concentration of species *i* in washcoat
L_c : characteristic length of washcoat
$Sh_{i\infty}$: asymptotic internal Sherwood number
R_i : internal mass transfer resistance
R_r : reaction resistance

Greek Symbols

ε : porosity for washcoat
τ : tortuosity
θ_i : site coverage for species *i*
ε_m : porosity of monolith reactors
Λ : constant related to the particle geometry

REFERENCES

1. E. Tronconi and P. Forzatti, *AIChE J.*, **38**, 201 (1992).
2. R. M. Heck, S. Gulati and R. J. Farrauto, *Chem. Eng. J.*, **82**, 149 (2001).
3. V. Khanaev, E. Borisova and A. Noskov, *Theor. Found. Chem. Eng.*, **39**, 478 (2005).
4. D. Chatterjee, T. Burkhardt, B. Bandl-Konrad, T. Braun, E. Tronconi, I. Nova and C. Ciardelli, *SAE transactions*, 2005-01-0965, 437 (2005).

5. D. Chatterjee, T. Burkhardt, M. Weibel, I. Nova, A. Grossale and E. Tronconi, *SAE Technical Paper* Series, 2007-01-1136 (2007).
6. E. Tronconi, I. Nova, C. Ciardelli, D. Chatterjee, B. Bandl-Konrad and T. Burkhardt, *Catal. Today*, **105**, 529 (2005).
7. A. Scheuer, O. Hirsch, R. Hayes, H. Vogel and M. Votsmeier, *Catal. Today*, **175**, 141 (2011).
8. P. Kumar, I. Makki, J. Kerns, K. Grigoriadis, M. Franchek and V. Balakotaiah, *Chem. Eng. Sci.*, **73**, 373 (2012).
9. C.-T. Chen and W.-L. Tan, *J. Taiwan Inst. Chem. Eng.*, **43**, 409 (2012).
10. M. Colombo, I. Nova, E. Tronconi, V. Schmeißer, B. Bandl-Konrad and L. Zimmermann, *Appl. Catal., B.*, **111**, 106 (2012).
11. Q. Su, L. Xie, S. Shuai, J. Wang, J. Song and Z. Li, *Catal. Today*, **216**, 292 (2013).
12. O. Deutschmann, L. Maier, U. Riedel, A. Stroemman and R. Dibble, *Catal. Today*, **59**, 141 (2000).
13. J. Kusaka, M. Sueoka, K. Takada, Y. Ohga, T. Nagasaki and Y. Daisho, *Int. J. Engine Res.*, **6**, 11 (2005).
14. J. Koop and O. Deutschmann, *SAE Technical Paper Series*, 2007-01-1142 (2007).
15. Z. Lei, X. Liu and M. Jia, *Energy Fuels*, **23**, 6151(2009).
16. B. W. Riyandwita and M.-W. Bae, *SAE Technical Paper Series*, 2011-01-1240 (2011).
17. B. Sawatmongkhon, A. Tsolakis, K. Theinnoi, A. York, P. Millington and R. Rajaram, *Appl.* Catal*., B.*, **111**, 165 (2012).
18. O. V. Ogidiama and T. Shamim, *Energy Procedia*, **61**, 2154 (2014).
19. F. Sadeghi, B. Tirandazi, A. Khalili-Garakani, S. Nasseri, R. N. Nodehi and N. Mostoufi, *Chem. Eng.* Res. *Des.*, **118**, 21 (2017).
20. C. Zheng, L. Xiao, R. Qu, S. Liu, Q. Xin, P. Ji, H. Song, W. Wu and X. Gao, *Chem. Eng. J.*, **361**, 874 (2019).
21. J. Braun, T. Hauber, H. Többen, J. Windmann, P. Zacke, D. Chatterjee, C. Correa, O. Deutschmann, L. Maier and S. Tischer, *SAE Technical Paper Series*, 2002-01-0065 (2002).
22. D. Chatterjee, O. Deutschmann and J. Warnatz, *Faraday Discuss.*, **119**, 371 (2002).
23. J. Windmann, J. Braun, P. Zacke, S. Tischer, O. Deutschmann and J. Warnatz, *SAE transactions*, 2003-01-0937, 713 (2003).
24. R. Holder, M. Bollig, D. Anderson and J. Hochmuth, *Chem. Eng. Sci.*, **61**, 8010 (2006).
25. S.-J. Jeong, W.-S. Kim and T. Kim, *Int. J. Veh. Des.*, **29**, 268 (2002).
26. W. Guojiang and T. Song, *Energy Convers. Manage.*, **46**, 2010 (2005).
27. R. Hayes, A. Fadic, J. Mmbaga and A. Najafi, *Catal. Today*, **188**, 94 (2012).
28. S. Tischer, C. Correa and O. Deutschmann, *Catal. Today*, **69**, 57 (2001).
29. P. Canu and S. Vecchi, *AIChE J.*, **48**, 2921 (2002).
30. A. Di Benedetto, G. Landi, V. Di Sarli, P. Barbato, R. Pirone and G. Russo, *Catal. Today*, **197**, 206 (2012).
31. M. Grimm and S. Mazumder, *Comput. Chem. Eng.*, **32**, 552 (2008).
32. G. Arzamendi, P. Diéguez, M. Montes, J. Odriozola, E. F. Sousa-Aguiar and L. Gandía, *Chem. Eng. J.*, **154**, 168 (2009).
33. X. Zhai, S. Ding, Y. Cheng, Y. Jin and Y. Cheng, *Int. J. Hydrogen Energy*, **35**, 5383 (2010).
34. L. Lao, A. Aguirre, A. Tran, Z. Wu, H. Durand and P. D. Christofides, *Chem. Eng. Sci.*, **148**, 78 (2016).
35. R. Ma, B. Castro-Dominguez, A. G. Dixon and Y. H. Ma, *Int. J. Hydrogen Energy*, **43**, 7662 (2018).
36. M. A. Ashraf, O. Sanz, C. Italiano, A. Vita, M. Montes and S. Specchia, *Chem. Eng. J.*, **334**, 1792 (2018).
37. J. von Rickenbach, F. Lucci, C. Narayanan, P. D. Eggenschwiler and D. Poulikakos, *Chem. Eng. J.*, **276**, 388 (2015).
38. R. Hayes, B. Liu and M. Votsmeier, *Chem. Eng. Sci.*, **60**, 2037 (2005).
39. M. Bhattacharya, M. P. Harold and V. Balakotaiah, *AIChE J.*, **50**, 2939 (2004).
40. S. Y. Joshi, M. P. Harold and V. Balakotaiah, *Chem. Eng. Sci.*, **65**, 1729 (2010).
41. N. Mladenov, J. Koop, S. Tischer and O. Deutschmann, *Chem. Eng. Sci.*, **65**, 812 (2010).
42. M. Irani, A. Alizadehdakhel, A. N. Pour, N. Hoseini and M. Adinehnia, *Int. J. Hydrogen Energy*, **36**, 15602 (2011).
43. Y. Du and P. W. Wang, *Int. J. Hydrogen Energy*, **39**, 3572 (2014).
44. M. E. Coltrin, R. J. Kee and F. M. Rupley, *Int. J. Chem. Kinet.*, **23**, 1111 (1991).
45. L. Olsson, K. Wijayanti, K. Leistner, A. Kumar, S. Y. Joshi, K. Kamasamudram, N. W. Currier and A. Yezerets, *Appl. Catal., B.*, **174**, 212 (2015).
46. M. M. Tomadakis and S. V. Sotirchos, *Chem. Eng. Sci.*, **48**, 3323 (1993).
47. L. Wu, V. Degirmenci, P. C. Magusin, N. J. Lousberg and E. J. Hensen, *J. Catal.*, **298**, 27 (2013).
48. S. Cordiner, G. De Simone and V. Mulone, *SAE Technical Paper Series*, 2007-01-4007 (2007).
49. M. J. Stutz and D. Poulikakos, *Chem. Eng. Sci.*, **63**, 1761 (2008).
50. A. Quiney, G. Germani and Y. Schuurman, *J. Power Sources*, **160**, 1163 (2006).
51. S. Chiuta, R. C. Everson, H. W. Neomagus, L. A. Le Grange and D. G. Bessarabov, *Int. J. Hydrogen. Energy*, **39**, 11390 (2014).
52. P. S. Metkar, M. P. Harold and V. Balakotaiah, *Chem. Eng. Sci.*, **87**, 51 (2013).
53. C. Depcik and D. Assanis, *Prog. Energy Combust. Sci.*, **31**, 308 (2005).
54. D. H. West, V. Balakotaiah and Z. Jovanovic, *Catal. Today*, **88**, 3 (2003).
55. S. Y. Joshi, M. P. Harold and V. Balakotaiah, *Chem. Eng. Sci.*, **64**, 4976 (2009).
56. V. Balakotaiah, *Chem. Eng. Sci.*, **63**, 5802 (2008).
57. D. Leung, R. Hayes and S. Kolaczkowski, *Can. J. Chem. Eng.*, **74**, 94 (1996).